# CrystEngComm

Over Melt Temperature

Cooling
Crystal Growth

Nucleation

ROYAL SOCIETY
OF CHEMISTRY | Celebrating
IYPT 2019

PAPER
Qiuliang Wang, Eric E. Hellstrom *et al.*
Investigation of the melt-growth process of YbBa$_2$Cu$_3$O$_{7-\delta}$ powder
in Ag-sheathed tapes

# Investigation of the melt-growth process of YbBa$_2$Cu$_3$O$_{7-\delta}$ powder in Ag-sheathed tapes†

Zili Zhang, [iD] [ab] Jianyi Jiang, [a] Hui Tian, [c] Qiuliang Wang, [*b] David C. Larbalestier [a] and Eric E. Hellstrom [*a]

We investigated the melt-growth behavior of YbBa$_2$Cu$_3$O$_{7-\delta}$ (Yb123) powder under different atmospheres for potential application in Ag-sheathed Yb123 wires. We chose Yb123 because it has the lowest melting temperature of the RE123 (RE = rare earth) phases. Yb123 needs to be melted under low oxygen partial pressure ($p$O$_2$) to depress its melt temperature below that of Ag. Here we report that adding Ag powder to Yb123 powder or encasing Yb123 powder in a Ag-sheath further decreases the melting temperature of Yb123. We designed a heat treatment process in which we varied the $p$O$_2$ during the heat treatment to melt the Yb123 in a Ag-sheathed powder-in-tube (PIT) wire and then regrow Yb123 on cooling. Based on these studies, we have developed a model for Yb123 melting and growth.

## Introduction

The high temperature superconductors (HTS) REBa$_2$Cu$_3$O$_{7-\delta}$ (RE123; RE = rare earth – also called REBCO), which have high current density ($J_c$), high irreversibility field ($H_{irr}$), and high critical transition temperature ($T_c$), have been successfully used in a number of applications including as inserts to high-field magnets,[1,2] transmission lines,[3,4] and fault current limiters.[5,6] To achieve high $J_c$, REBCO has to be deposited as a thin film on a flat, highly-textured substrate. Fabricating this coated conductor (CC) tape geometry requires complex processing to create a biaxially-textured REBCO film that allows the supercurrent to flow across low-angle grain boundaries of typically <5° misorientation.[7,8,9] The two most common methods to achieve the required bi-axial texture are ion beam assisted deposition (IBAD) and rolling assisted biaxially textured substrate (RABiTS),[10] both of which require depositing multiple layers of different materials before the REBCO is deposited. These deposition routes are complex and expensive, so REBCO CC is too costly for many applications.[11]

It would be useful for REBCO applications if it were possible to fabricate high-$J_c$ REBCO conductors using the simpler powder-in-tube (PIT) method to make a flat tape or preferably a round wire. The PIT route is used to fabricate Bi-2223 (Bi$_2$Sr$_2$Ca$_2$Cu$_3$O$_{10}$) tape and Bi$_2$Sr$_2$CaCu$_2$O$_8$ (Bi-2212) round wire.[12,13] Bi-2212 is particularly interesting because when Ag-sheathed Bi-2212 wire is heat treated, it naturally grows a biaxially-aligned microstructure during cooling with high $J_c$.[14] We use Bi-2212 as our model for what we would like to achieve with REBCO: being able to make a PIT REBCO conductor that grows highly-aligned, well-connected, high-$J_c$ REBCO grains from the melt during the heat treatment. Like Bi-2212, we think that Ag is the only viable sheath material for PIT REBCO wires because it does not react with or poison REBCO, it is not oxidized at high temperature, and it is permeable to oxygen, so that the oxygen content, and thus doping state, of the REBCO can be controlled to optimize the superconducting properties.

Prior attempts have been made to fabricate high $J_c$ REBCO wires using the PIT method, but they did not yield high $J_c$.[15–22] The highest critical current ($I_c$) was only 3300 A cm$^{-2}$ at 77 K self-field.[23] We evaluated REBCO melt-growth techniques used to grow single crystals from the melt state, which include the MTG (melt textured growth[24]), QMG (quench and melt growth[25]), and MPMG (melt powder melt growth routes[26]). But, these processes are not particularly relevant for Ag-sheathed REBCO conductors because most of the REBCOs melt far above the melting temperature of Ag.

To melt REBCO in Ag, the melting temperature of REBCO has to be below that of Ag. For this study we chose Yb123,

$^a$ *Applied Superconductivity Center, National High Magnetic Field Laboratory, Florida State University, Tallahassee, FL 32310, USA.*
*E-mail: hellstrom@asc.magnet.fsu.edu*
$^b$ *Institute of Electrical Engineering, Chinese Academy of Sciences (CAS), Beijing 100190, China. E-mail: wongsm17@mail.iee.ac.cn*
$^c$ *Key laboratory for Thermal Science and Power Engineering of Ministry of Education, Department of Thermal Engineering, Tsinghua University, Beijing, 100084, China*

which has the lowest melting temperature of the REBCOs (975 °C in 1 atm $O_2$).[27] Previous studies showed that changing the partial pressure of oxygen ($pO_2$) in the ambient atmosphere changes both the melting temperature of $YBa_2Cu_3O_{7-\delta}$ (Y123) and of Ag.[28] Our goal in the present study was to develop a heat treatment process to melt Yb123 powder below the melting temperature of Ag and then grow Yb123 grains in a Ag-sheathed Yb123 wire, and to investigate the phase purity and microstructure of the Yb123 that grew in the PIT wire.

In this paper, we report on the melt temperature of Yb123 under different $pO_2$ and the effect of Ag on its melting temperature. We designed a heat treatment that varies the $pO_2$ and temperature to melt and grow Yb123 in a Ag sheath. This study provides an important potential starting point to develop an alternative route for fabricating REBCO wires and tapes.

## Experimental

### Powder preparation

Yb123 powder was synthesized by a solid-state reaction. $Yb_2O_3$ (99.99% Alfa Aesar), $BaCO_3$ (99.8% Baker Analyzed) and CuO powder (99.995% Alfa Aesar) were mixed to give the stoichiometric 1 : 2 : 3 Yb : Ba : Cu ratio, ground together, and pressed into a pellet that was put into a tube furnace and heat treated at 920 °C for 24 h under flowing $O_2$. The pellet was ground to fine powder and X-rayed to follow the extent of reaction. This process was repeated until the powder was pure Yb123 by X-ray analysis. After the final heat treatment, the critical transition temperature ($T_c$) of Yb123 powder was measured as shown in Fig. S1 in the ESI.†

### Tape preparation

The Yb123/Ag tape was fabricated by the powder-in-tube (PIT) method. Pure, as-synthesized Yb123 powder was packed into Ag tubes (OD: 6.35 mm; ID: 4.35 mm) that were sealed on one end. After a tube was packed with powder, its open end was sealed, it was drawn down to 4.62 mm diameter and then rolled with 10% reductions in thickness into a flat tape 1.02 mm thick whose ceramic core thickness was around 400 μm. These Ag-sheathed Yb123 samples are called tapes because they are flat.

### Heat treatment to study melting and growth of Yb123

To study the melting of Yb123 powder, we pressed as-synthesized powder into round pellets and placed them in $Al_2O_3$ boats for heat treatment. For the Ag-sheathed Yb123 samples, we cut the tape into 10 cm long sections that were also heat treated in $Al_2O_3$ boats. All heat treatments were done in a tube furnace with a removable quartz muffle tube that was only used for this Yb123 study. Before heating, Ar was flowed through the muffle tube at a high flow rate for an extended period to replace the air in the tube with Ar. After the tube was flushed, the Ar flow rate was reduced and the heat treatment was started. The details of the specific heat treatment schedules and the results from each heat treat-

ment are given in the Results section. During the heat treatments, we changed the temperature and also changed the atmosphere in the furnace from Ar to $O_2$ by flowing $O_2$ into the muffle tube to replace the Ar. The details of changing from Ar to $O_2$ for specific heat treatment schedules are also given in the Results section.

After we found that Ag affected the melting temperature of Yb123, we investigated whether Ag also affected the melting temperature of other REBCO compounds. To investigate this, we mixed Y123 and Er123 powder with Ag powder and did DTA (differential thermal analysis) (TA Instruments 2960) studies in flowing $O_2$.

To investigate melting and growth of Yb123, we compared pellets of Yb123 and Bi-2212 powder after they had been melted in an $Al_2O_3$ boat. The Bi-2212 pellets were heated in flowing $O_2$ with the same flow rate used for Yb123. The Bi-2212 pellet was heated to 890 °C at 600 °C h$^{-1}$ in pure $O_2$, held for 2 h and furnace cooled to room temperature. The Yb123 pellet was heated to 985 °C at 600 °C h$^{-1}$ in $O_2$, held for 2 h and furnace cooled to room temperature.

### Sample characterization

The phase analysis of the samples was characterized by Cu Kα X-ray diffraction (XRD) using a Philips goniometer. For the tape samples, ceramic material was extracted from the tape after heat treatment and ground into a powder. Microstructures were observed by scanning electron microscopy (SEM, Zeiss EsB in lens) with elemental analysis performed by energy dispersive X-ray (EDX) analysis. DTA was used to determine the melting temperature of powders and Ag-sheathed Yb123 in different atmospheres. The DTA heating rate of 600 °C h$^{-1}$ was the same as that used in the actual heat treatments in this study. The field-cooled and zero-field-cooled dc susceptibility was measured in an MPMS (Quantum Design) under an applied field of 10 mT.

## Results

In this Results section, we present results from specific experiments plus the logic we used to design these experiments. We include our logic because we were not able to develop as much melt in the wire as we desired and we think this guidance can help future investigators develop other ways to achieve more liquid in the melt state.
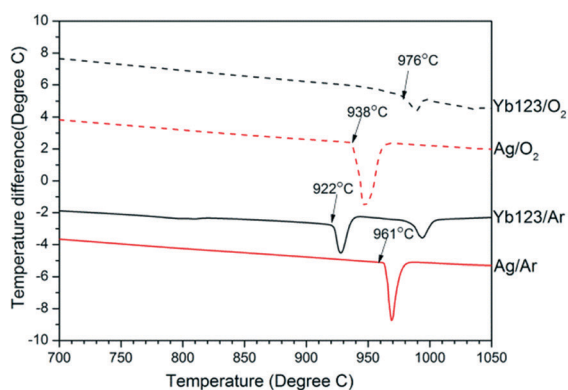
### (a) Melting of Yb123

Fig. 1(a) shows DTA curves of Yb123 powder and Ag heated in $O_2$ and Ar. In 1 atm $O_2$, Yb123 melts at 976 °C, which is higher than the melting temperature of Ag in 1 atm $O_2$ (938 °C). However, in 1 atm Ar, the melting temperature of Yb123 decreases to 922 °C, whereas the melting temperature of Ag is 961 °C in Ar. This suggests that it should be possible to melt Yb123 in a Ag-sheathed Yb123 wire under pure Ar. In this paper, we refer to the downward-pointing peaks in the DTA runs, as in Fig. 1(a), simply as peaks. The second peak

in the Yb123/Ar curve around 986 °C is the reaction between Yb$_2$BaCuO$_5$ (Yb211) and CuO.[29]
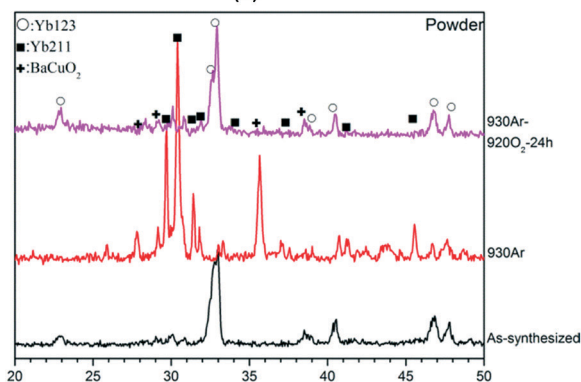
Fig. 1(b) shows XRD patterns of Yb123 powders that were melted in Ar at 930 °C, which is 31 °C below the melting temperature of Ag, and were then heat treated in different ways to try to regrow Yb123 from the melt. In one experiment (labelled 930Ar), a pellet of Yb123 powder was heated to 930 °C, held for 2 h, and then cooled to room temperature in flowing Ar. The XRD pattern shows that, after cooling in Ar, the sample contained mainly Yb$_2$BaCuO$_{5-\delta}$ (Yb211) that was present in the melt, BaCuO$_2$, which had formed from the unreacted liquid as it cooled, and only a very small amount of Yb123. This validates that Yb123 melts in Ar at 930 °C, but more importantly, it shows that Yb123 does not grow from the melt in an Ar atmosphere. These results show that the melting reaction given by reaction (1) is the same in Ar and O$_2$.[29]

$$YbBa_2Cu_3O_{7-\delta} \rightarrow Yb_2BaCuO_{5-\delta} + L \qquad (1)$$

L is liquid. We use the word melt to indicate forming some liquid phase on heating, and we also use it to indicate the mixture of liquid plus crystalline phases that form when Yb123 melts, as shown in reaction (1). In the heat treatment labelled 930Ar–920O$_2$-24 h in Fig. 1(b), we changed the atmosphere from Ar to O$_2$ after melting and also changed the temperature to attempt to regrow Yb123 from the melt. The sample was heated to 930 °C and held for 2 h in Ar, cooled to 920 °C while the atmosphere was simultaneously changed from Ar to O$_2$, held at 920 °C for 24 h in flowing O$_2$, and then cooled to room temperature. The XRD result shows the main phase was Yb123 with only small amounts of Yb211 and BaCuO$_2$. This indicates that Yb123 can be melted in Ar but the $pO_2$ has to be increased (in our studies we used 1 atm O$_2$) to grow Yb123 from the melt. The amount of each phase in the X-ray patterns is summarized in Table S1 in the ESI.†

Based on the results shown in Fig. 1, we designed the heat treatment shown in Fig. 2(a) for Ag-sheathed Yb123 tape. Fig. 2(a) has three lines in it: a solid line (red) for the heating schedule, a dashed line (blue) for the furnace atmosphere, and a dash-dot line (green) that shows the expected phases



(a)
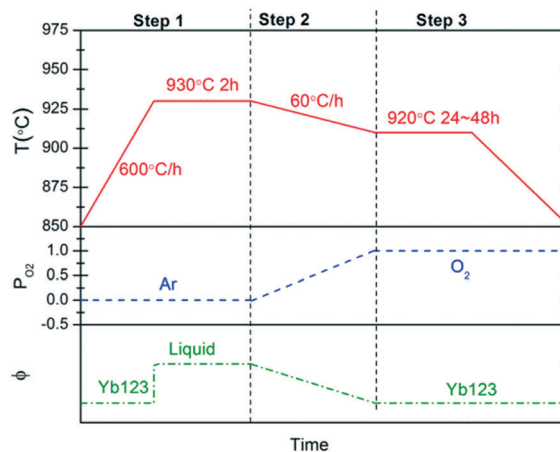


(b)

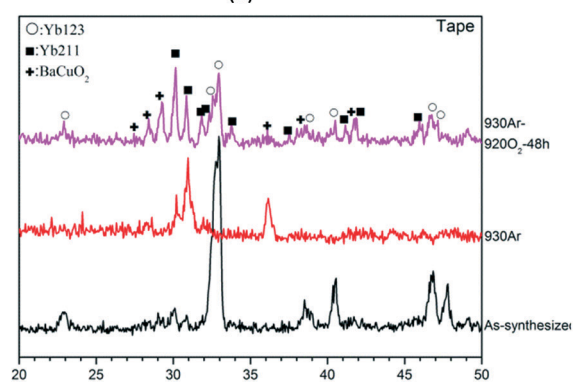Fig. 1 (a) The DTA results of Yb123 and Ag powder heated under Ar (solid lines) and O2 (dashed lines). (b) The XRD patterns of (1) as-synthesized Yb123 powder, (2) after melting and cooling Yb123 powder in Ar (labelled 930Ar) and (3) after melting Yb123 powder in Ar at 930 °C and holding at 920 °C in O$_2$ for 24 h before cooling (labelled 930Ar–920O$_2$-24 h). Arrows in the DTA curves in (a) indicate the melting temperature.



(a)



(b)

Fig. 2 (a) The heat treatment process designed for Ag-sheathed Yb123 tape based on the DTA results in Fig. 1. The three $y$ axes from top to bottom are temperature (red solid line), $pO_2$ (blue dash line), and phases (green dash-dot line). (b) XRD patterns of as-synthesized Yb123 powder, the ceramic core of the Ag-sheathed Yb123 tape after step 1 (930Ar), and the ceramic core after the entire heat treatment (930Ar–920O$_2$-48 h).

in the tape. The heat treatment consists of three steps. In step 1 the sample is heated to 930 °C at 600 °C h$^{-1}$ and held for 2 h in Ar to melt the Yb123. In step 2 the temperature is decreased to 920 °C at 60 °C h$^{-1}$ while the flowing Ar is replaced by flowing O$_2$. Step 3 holds the sample at 920 °C for 24 to 48 h, followed by furnace cooling to room temperature in about 4 h.

Fig. 2(b) shows the XRD patterns of an as-synthesized Yb123 powder, at the end of step 1 after melting the Yb123 (labelled 930Ar – sample was cooled to room temperature in Ar), and after the entire heat treatment (labelled 930Ar–920O$_2$-48 h). The XRD patterns show that the Yb123 powder in the Ag-sheathed Yb123 tape melted in step 1, and that a small amount of Yb123 grew while at 920 °C for 48 h in O$_2$ in step 3 (see Fig. 2(b)). Because we used the same Yb123 powder in the studies shown in Fig. 1(b) and 2(b), we speculate that the smaller amount of Yb123 that grew in the Ag-sheathed Yb123 tape (Fig. 2(b)) compared to the larger amount of Yb123 in the pellet (Fig. 1(b)) is due to interactions with Ag in the tape.

We then did DTA studies to determine the effect Ag has on melting Yb123, which is shown in Fig. 3. The experiments used pure, as-synthesized Yb123 powder, Yb123 powder mixed with Ag powder (Alfa Aesar), or a Ag-sheathed Yb123 PIT tape. The samples shown 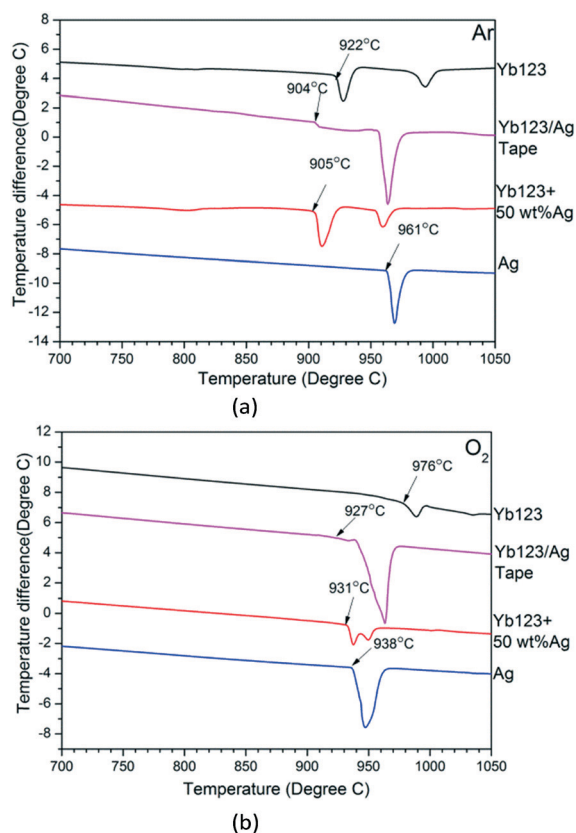in Fig. 3(a) and (b) were heated in flowing Ar and O$_2$, respectively. Fig. 3(a) shows that adding Ag powder depresses the melting temperature of Yb123 to 905 °C in Ar compared to 922 °C for as-synthesized Yb123 powder in Ar. Fig. 3(b) shows that mixing Ag powder into Yb123 powder also decreases the melting temperature of Yb123 from 976 °C to 931 °C in pure O$_2$. The melting temperature of Yb123 in the Ag-sheathed Yb123 tape sample under Ar and O$_2$ showed very similar melt temperatures to Yb123 mixed with Ag powder and heated in Ar or O$_2$. The Yb123 melting temperatures in Ar are 904 °C in tape and 905 °C mixed with Ag powder, and in O$_2$ they are 927 °C in tape and 931 °C mixed with Ag powder. In the Ag-sheathed Yb123 sample, the Ag sheath surrounded the Yb123 ceramic core but was not mixed with the Yb123 powder. Nevertheless, just having Ag surround the Yb123 powder depressed the melt temperature of Yb123 just the same as mixing Ag with Yb123 powder.

We did not find prior studies in the literature showing that Ag decreases the melting temperature of RE123 compounds, so we tested YBa$_2$Cu$_3$O$_{7-\delta}$ (Y123) and ErBa$_2$Cu$_3$O$_{7-\delta}$ (Er123) in contact with Ag powder. As shown in Fig. S2 and S3,† Ag decreases the melting temperature of Y123 and Er123, just as it does for Yb123.

The melt temperatures for Yb123, Y123 and Er123 are summarized in Table S2 in the ESI.†

Fig. 4 plots the melt temperatures of mixtures of Yb123 and Ag powder from DTA runs as a function of the amount of Ag in the mixture. Adding as little as 5 wt% Ag decreases the melting temperature of Yb123 from 976 °C to 931 °C under pure O$_2$; however, the melting temperature of Yb123 does not decrease significantly with additions of more than ~5 wt% Ag.

### (b) Growth of Yb123

After studying the melt behaviour of Yb123, we investigated the growth behaviour of Yb123 from the melt. We believe that step 2 in the heat treatment (see Fig. 2(a)) is critical to growing Yb123 on cooling, and it is also challenging, because



**Fig. 3** DTA results for pure Yb123 powder, Yb123 + 50 wt% Ag powder, Ag-sheathed Yb123 tape, and pure Ag powder in (a) Ar and (b) O$_2$. The arrow shows the melting temperature of the sample.



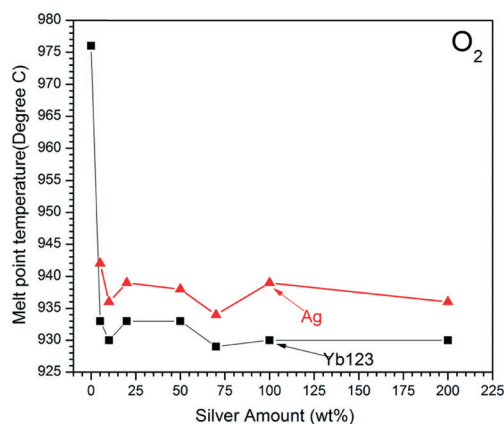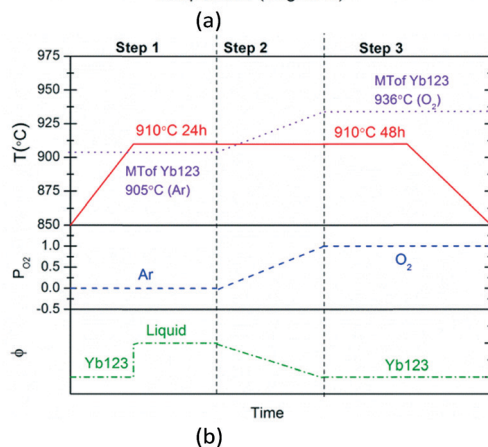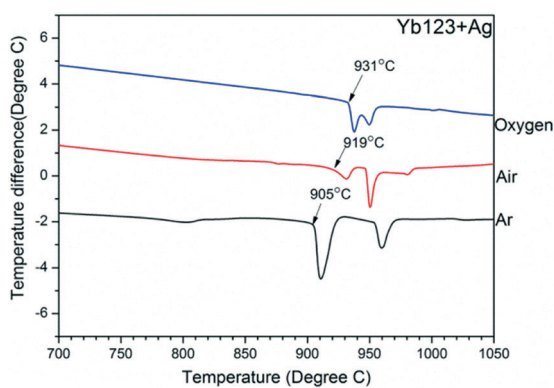**Fig. 4** The melt temperature of Yb123 plus Ag powder as a function of the amount of Ag in the mixture measured in flowing O$_2$.
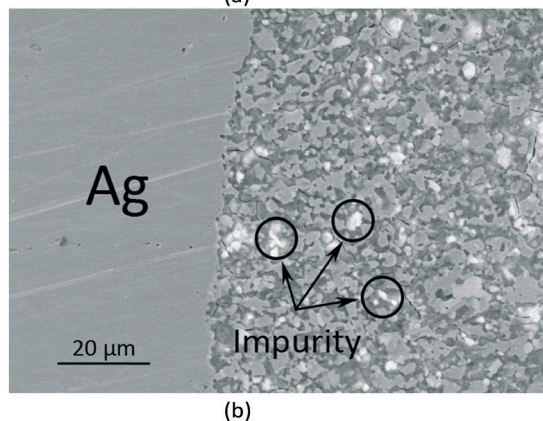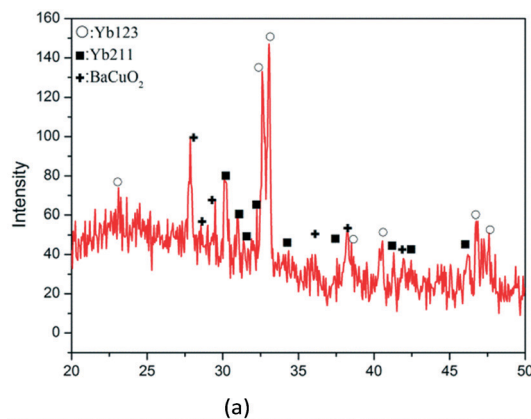
during step 2 in Fig. 2(a) the temperature and $pO_2$ are simultaneously changing. We changed from Ar to $O_2$ in Step 2 because Yb123 needs high $pO_2$ to grow. We decreased the temperature in step 2 to allow Yb123 to nucleate and grow. An additional complicating factor is that the melting temperature of Yb123 increases as the $pO_2$ increases during step 2, as shown in Fig. 5(a).

Based on the results shown in Fig. 4 and 5(a), we modified the heat treatment shown in Fig. 2(b) to that shown in Fig. 5(b). The heat treatment in Fig. 5(b) heated the Ag-sheathed Yb123 tape to 910 °C in Ar, just above the melting temperature of Yb123 in Ar, and held the temperature at 910 °C as the gas was changed from Ar to $O_2$ (step 2) to increase the melting temperature of Yb123. In step 3, the tape was held for 48 h at 910 °C in $O_2$ before cooling to room temperature to allow the Yb123 to grow from the melt. Only having to change the gas and not the temperature in step 2 simplifies control of the heat treatment process.

The XRD results in Fig. 6(a) show the phases present after the heat treatment in Fig. 5(b). They show more Yb123 formed than in the heat treatment of Fig. 2(b). The two sharp peaks at 32.61° and 33.05° correspond to the (103) and (013) peaks of tetragonal Yb123. However, there are also some
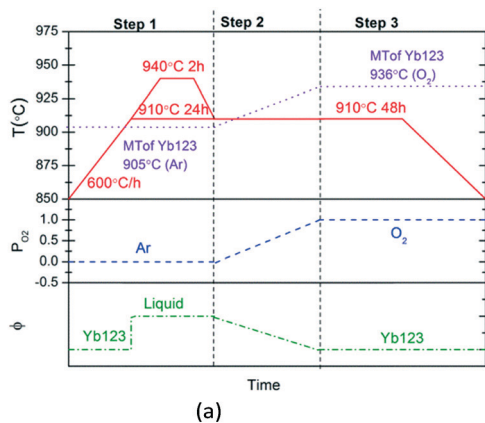


(a)



(b)

**Fig. 6** (a) XRD results and (b) secondary electron SEM image of a transverse cross section of Ag-sheathed Yb123 tape after the heat treatment in Fig. 5(b). The circled grains in (b) are Yb211.
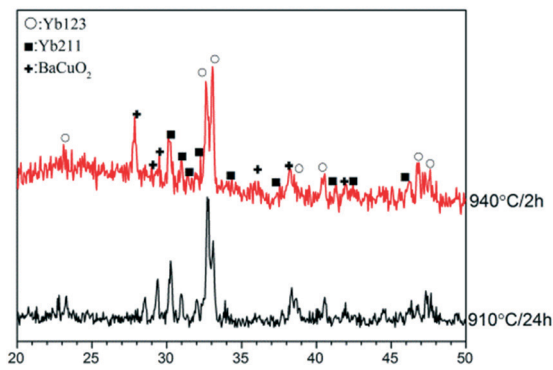
peaks from the unwanted Yb211 and $BaCuO_2$ phases in the pattern. Fig. 6(b) is an SEM image of a transverse cross section of the Ag-sheathed Yb123 tape after the heat treatment in Fig. 5(b). There are many small grains 3 to 5 μm in size (circled) that EDX showed to be Yb211. These unwanted phases are surrounded by grains of Yb123 that are ~10 μm in size. The small, homogenously-distributed, unwanted particles mixed with the Yb123 grains block the physical connectivity of Yb123 grains, which may be a significant barrier to supercurrent flow.

To eliminate these unwanted phases, the heat treatment needs to be further optimized. We thought that a possible reason for unwanted remnant phases was that, during the growth step, the Yb211 grains were so large that they could not fully react to form Yb123 during cooling. Reaction (1) shows Yb211 forms on melting, and it could have grown to large size when holding the samples for extended time (24 h at 910 °C) during step 1 (see Fig. 5(b)).

To address this possibility, we designed the heat treatment in Fig. 7(a). Here we investigated several different temperatures and times in step 1: two are shown in Fig. 7(a) (910 °C for 24 h, and 940 °C for 2 h then cooled to 910 °C) to try to form Yb211 with different grain size. The XRD results (Fig. S4†) showed that Yb123 completely melted to Yb211 and liquid for the temperatures and times used in step 1. After the



(a)



(b)

**Fig. 5** (a) DTA results of Yb123 + 50 wt% Ag powder under atmospheres with different $pO_2$. (b) Heat treatment process for melt-growth of Ag-sheathed Yb123 tape. Steps 1–3 were all done at 910 °C and the gas was changed from Ar to $O_2$ in step 2. In (b), the dotted line labelled MT is the melting temperature of Yb123, and the other lines are explained in Fig. 2.
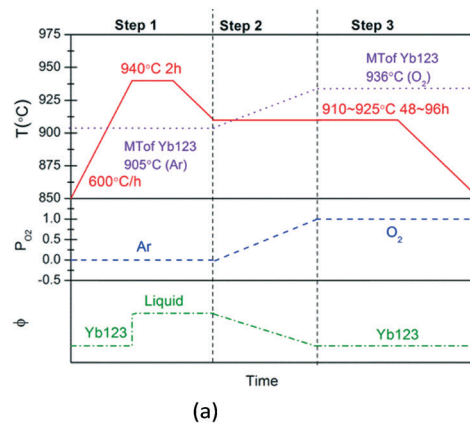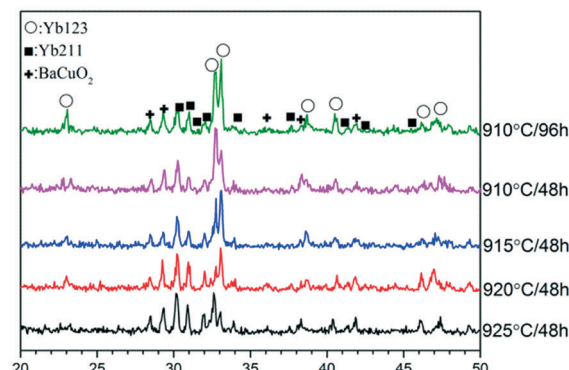
(a)



(b)

**Fig. 7** (a) Two different heat treatment processes with different melt temperatures and times in step 1. (b) XRD results for Ag-sheathed Yb123 samples with different times and temperatures during step 1. MT with the dotted line in (a) means the melt temperature of Yb123. The lines in (a) are explained in Fig. 2 and 5.



(a)



(b)

**Fig. 8** (a) Heat treatment where the temperature is varied in steps 2 and 3, and the time is varied in step 3. (b) XRD results of Ag-sheathed Yb123 for different temperatures and times in step 3. MT with the dotted line in (a) means the melt temperature of Yb123. The lines in (a) are explained in Fig. 2 and 5.

complete heat treatment, the XRD results (Fig. 7(b)) showed that Yb123 is the main phase in both samples. However, there is no obvious difference in the amount of unwanted phases between the two samples with different times and temperatures in step 1. This result indicates that our hypothesis about growing large grains of Yb211 in the melt that prevent forming Yb123 is wrong.

We refined the heat treatment further as shown in Fig. 8(a) to try to reduce further the unwanted phases by optimizing the time and temperature in step 3 where Yb123 continues to nucleate and grow. As before, the gas was changed from Ar to $O_2$ in step 2. The temperature in steps 2 and 3 was kept constant in this study, and was varied from 910 °C to 925 °C for times from 48 to 96 h. The XRD patterns in Fig. 8(b) show that the amount of unwanted phases increases with increasing temperature in steps 2 and 3, with the 910 °C and 915 °C samples having the most Yb123. The maximum amount of Yb123 formed at 910 °C. Normally, increasing the heat treatment time increases the extent of reaction, so the time at 910 °C was increased to 96 h, but as the XRD results in Fig. 8(b) show, increasing the time to 96 h did not increase the Yb123 content, so 48 h at 910 °C is long enough to form Yb123 in step 3. These optimization studies indicate that the

unwanted phases are not due to heat treatment parameters. Further possible reasons for still having unwanted phases present are presented in the Discussion.

The results of the experiments comparing the melting of Yb123 and Bi-2212 pellets are shown in Fig. 9. During the heat treatment, the Bi-2212 sample slumped (Fig. 9(a)), and it had a smooth, glistening surface indicating much liquid present in the melt state. In contrast, the Yb123 sample (Fig. 9(b)) did not slump much and it had a rough, matte surface suggesting much less liquid in the Yb123 melt.

## Discussion

Fabricating a superconducting Ag-sheathed REBCO wire requires that the REBCO powder can melt and grow inside the



(a) (b)

**Fig. 9** Light micrographs of (a) Bi-2212 (890 °C/2 h) and (b) Yb123 pellets (915 °C/2 h) after melting and rapid cooling to room temperature in flowing $O_2$.

Ag sheath, so it must melt at a lower temperature than Ag. For this study we chose Yb123, which has the lowest melting temperature of the REBCO compounds. As shown in Fig. 1(a), the melting temperatures of Ag and Yb123 vary with $pO_2$, the melting temperature of Yb123 increases and of Ag decreases with increasing $pO_2$. In 1 atm $O_2$, Yb123 melts at a higher temperature than Ag, so a Ag-sheathed Yb123 wire cannot be melt processed in 1 atm $O_2$. However, replacing $O_2$ by Ar depresses the melting temperature of Yb123 while simultaneously increasing the melting temperature of Ag, making it possible to melt Yb123 inside a Ag sheathed wire.

In addition to $pO_2$ affecting the melting temperatures, Fig. 3 shows that Ag in contact with Yb123 decreases the melting temperature of Yb123 both when Yb123 powder is mixed with Ag powder and when Yb123 powder is surrounded by a Ag sheath. This is fortuitous because the melting temperature decreases from adding Ag to Yb123 and from melting Yb123 in Ar are additive, resulting in a melting temperature of Yb123 in contact with Ag in Ar that is ~905 °C, which is ~56 °C lower than the melting temperature of Ag in Ar. This decrease in melting temperature in the presence of Ag powder or in a Ag sheath is also seen in Bi-2212 and Bi-2223.[30] Based on the melting depression of Yb123, Y123, and Er123 powders mixed with Ag powder, we suggest that Ag decreases the melting temperature of all of the REBCOs.

It has been suggested that when Ag is heated on RE123 at high temperatures, a layer of oxygen-saturated silver forms by direct reaction with $O_2$ from the atmosphere or by redox reaction with RE123.[31] The molten Ag wets and penetrates the RE123 ceramic, perhaps enhanced by formation of the Ag–O eutectic composition. Surface spreading occurs more rapidly at higher $p(O_2)$ because oxygen is more readily available. With longer heating times the Ag–O liquid partially reduces RE123 to RE211, $BaCuO_2$, and oxygen – so with saturated Ag–Cu alloy near the interface, the reaction formula could be as below:

$$RE123 + Ag\text{–}O(\text{eutectic liquid}) = RE211 + BaCuO_2 + Ag\text{–}Cu\text{–}O(\text{liq}) + O_2(g).$$
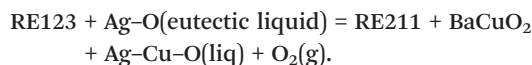
Says this mechanism can also explain why the Ag tape can affect the melt temperature of Yb123 as mixing powder. The Ag in the inner side of tape is first to form Ag–O eutectic liquid and it can diffuse to Yb123. This mechanism can explain why the Ag sheath remains solid but successfully affects the Yb123 core inside the tape.

After we were able to melt Yb123 in Ag-sheathed tape, we tried to devise a heat treatment to grow the Yb123 from the melt. As Fig. 2(b) shows, Yb123 growth requires an $O_2$ atmosphere.

Although we could melt Yb123 in a Ag sheath in Ar, no Yb123 grew from the melt when it was cooled in Ar (Fig. 1(b)). To grow Yb123 in the Ag sheath, we had to increase the $pO_2$ enough that Yb123 would form while not simultaneously decreasing the melting temperature of Ag so much that it would melt. We could prevent Ag from melting

by keeping the temperature below 938 °C, which is the melting point of Ag in 1 atm $O_2$. As shown in Fig. 2, we simultaneously decreased the temperature and increased the $pO_2$ to grow Yb123 from the melt. XRD showed this procedure formed some Yb123 but the sample contained a large volume fraction of impurity phases. Ideally, we want to go slowly through the thermodynamic point where Yb123 begins to form so the system forms a few Yb123 nuclei that grow to large size. However, with our experimental setup we could not accurately and reproducibly coordinate the change from pure Ar to pure $O_2$ with the change in temperature, so we looked for a simpler heat treatment to grow Yb123 from the melt.

A simpler method was to hold the temperature constant and only change the $pO_2$. We set the temperature in steps 1 through 3 at 910 °C, which is below the melting point of Ag in pure $O_2$, and changed from pure Ar to pure $O_2$ (see Fig. 5). Changing from Ar to pure $O_2$ increased the melting temperature of Yb123 in contact with Ag from 905 to 931 °C. XRD patterns (Fig. 6(a)), show that this procedure grows Yb123, but there is still a large fraction of impurity phases in the product.

Having developed the ability to grow Yb123 from the melt by changing $pO_2$, the next set of experiments explored increasing the amount of Yb123 that grew from the melt. Based on microstructural images like Fig. 6, we hypothesized that large grains of Yb211 formed in the melt during step 1, which hindered growth of Yb123 according to the reverse of reaction (1). The heat treatment in Fig. 7 shortened the time in step 1 before starting to form Yb123 in step 2, to try to prevent forming large grains of Yb211. XRD showed about the same amount of impurity phases in the final product, indicating either that large Yb211 formed in shorter times than we used in the Fig. 7 studies, or that other factors limit growth of Yb123 from the melt.

We also studied whether allowing more time or increasing the reaction temperature in step 3 when growing Yb123 (see Fig. 8) would increase the amount of Yb123 that formed. None of the combinations of time and/or temperature we used in step 3 significantly increased the amount of Yb123 that grew in the tape.

The guiding principle of our study was to try to find experimental conditions that would allow us to melt and grow Yb123 in a Ag-sheathed wire like is done in Ag-sheathed Bi-2212 wires.[32] We successfully melted Yb123 in a Ag sheath; however, unlike Bi-2212, very little Yb123 grew from the melt on cooling, and we believe that this Yb123 was not well aligned. The poor alignment may have been because the Yb123 core was several hundred micrometers thick, which, based on Bi-2212 studies, is too thick to texture the Bi-2212, which only self-aligns in thin 2D planes or narrow 1D filaments.[14] Fig. 9 highlights a significant difference between Yb123 and Bi-2212 in the melt state. There appears to be much more liquid in the Bi-2212 melt than in the Yb123 melt. This difference in amount of liquid is important in the model we have developed and describe below.
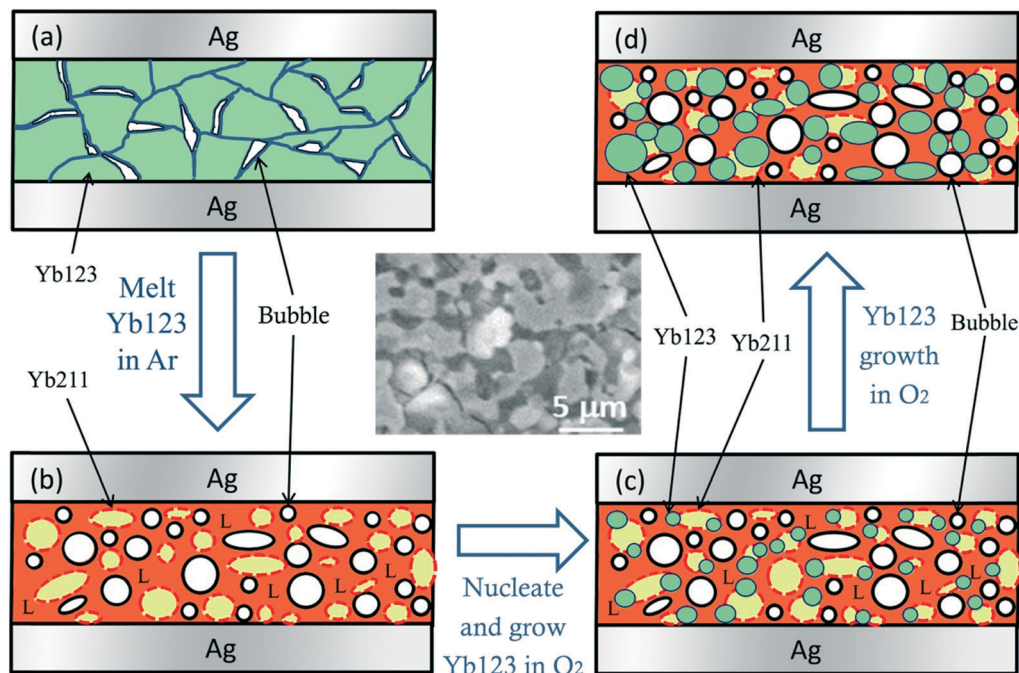
**Fig. 10** The model of the melt-growth process of Yb123 resulting in microstructure with a homogeneous distribution of impurity phases. See the text for a detailed description of this growth model. The white circles represent gas bubbles, the green circles represent Yb123, the yellow circles represent Yb211, and the red region represents liquid phase and $BaCuO_2$. The (a) to (d) show the four stage of the melt-growth process, which are initial stage (a), melt stage (b), nucleation stage (c) and growth stage (d). The SEM image in the center shows the final microstructure.

Based on our results, we propose a model for growth of Yb123 from the melt shown in Fig. 10. In the as-rolled Ag-sheathed Yb123 PIT tape, shown in Fig. 10(a), grains of Yb123 are encased in the Ag sheath with a packing density that is about 65–70%.[33] The space between the grains of Yb123 is filled with air.

When the Yb211 melts, reaction (1) shows that the melt consists of liquid and Yb211. In addition, air bubbles are present in the melt because the powder in the PIT tape is not 100% dense, and the air that surrounds the grains of Yb123 agglomerates, forming large bubbles. Thus, the melt actually consists of liquid (L in the figure), Yb211 (yellow circles), and gas bubbles (white circles), as shown in Fig. 10(b).

When Yb123 begins to grow from the melt by decreasing the temperature or increasing the $pO_2$, Yb123 grows by the reverse of reaction (1), which is liquid plus Yb211 going to Yb123. Although we do not know the details of this peritectic-type reaction, we know that cations from the liquid and cations from Yb211 need to combine to form Yb123. We expect that the interface between the Yb211 particles and liquid has the lowest nucleation energy, so we hypothesize that Yb123 forms at the surface of Yb211 in contact with the liquid (as shown by the green circles). The liquid provides a rapid diffusion pathway for the cations, but this pathway is limited because only a relatively small amount of liquid forms in the melt. As Yb123 grows, the amount of liquid decreases reducing the cation pathway. In addition, the gas bubbles block cation motion in the liquid reducing the amount of Yb123 that grows and the new

Yb123 grains that form also block the cation pathways in the liquid, preventing additional Yb123 growth. This is shown in Fig. 10(c) where some Yb123 has formed. With increasing time, more Yb123 grows, but not all of the liquid and Yb211 is consumed, as shown in Fig. 10(d). The final microstructure after the full heat treatment, shown in Fig. 6(b) and the SEM image in the middle of Fig. 10, consists of Yb123, Yb211, $BaCuO_2$, and bubbles.

## Conclusions

We systematically investigated the melt-growth behavior of Yb123 and were able to melt and then grow Yb123 in a Ag sheath. This requires changing the $pO_2$ during the heat treatment. Initially the $pO_2$ has to be low (we used Ar) so the Yb123 melts below the melting temperature of Ag, and then the $pO_2$ has to be increased (we used 1 atm $O_2$) to grow Yb123 from the melt. We found that Ag depresses the melting temperature of Yb123, and we also think it depresses the melting temperature of all the RE123s. It is advantageous that Ag depresses the melting temperature of Yb123 because this decrease in melting temperature creates a bigger difference in temperature between the melting temperature of Yb123 and the Ag sheath. Only a limited amount of Yb123 grew from the melt, which may due to the small amount of liquid that forms in the melt combined with the blocking effect of the Yb211 and bubbles in the melt that hamper Yb123 growth, which we describe in a grain-growth model.

## Conflicts of interest

There are no conflicts to declare.

## Acknowledgements

## Notes and references

1 X. Wang, S. Caspi, D. R. Dietderich, W. B. Ghiorso, S. A. Gourlay, H. C. Higley, A. Lin, S. O. Prestemon, D. van der Laan and J. D. Weiss, *Supercond. Sci. Technol.*, 2018, **31**, 045007.
2 J. Liu, Y. Dai and L. Li, *Cryogenics*, 2016, **79**, 79–84.
3 X. H. Zong, D. Wei, Y. Han and T. Tang, *IEEE Trans. Appl. Supercond.*, 2016, **26**, 5403404.
4 N. Bykovsky, D. Uglietti, K. Sedlak, B. Stepanov, R. Wesche and P. Bruzzone, *Supercond. Sci. Technol.*, 2016, **29**, 084002.
5 C. A. Baldan, W. Yuan, C. Y. Shigue and E. R. Filho, *IEEE Trans. Appl. Supercond.*, 2016, **26**, 5401905.
6 M. Majka, J. Kozak and S. Kozak, *IEEE Trans. Appl. Supercond.*, 2017, **27**, 5601405.
7 D. Dimos, P. Chaudhari and M. Mannhart, *Phys. Rev. B: Condens. Matter Mater. Phys.*, 1990, **41**, 4038–4049.
8 Y. Zhao, P. Torres, X. Tang, P. Norby and J.-C. Grivel, *Inorg. Chem.*, 2015, **54**, 10232–10238.
9 Y. Zhao, W. Wu, X. Tang, N. Andersen, Z. Han and J.-C. Grivel, *CrystEngComm*, 2014, **16**, 4369–4372.
10 Y. Zhao, H. Suo, Y. Zhu, J.-C. Grivel, M. Gao, L. Ma, R. Fan, M. Liu, Y. Ji and M. Zhou, *Acta Mater.*, 2009, **57**, 773–781.
11 M. Rupich and X. Li, *Phys. C*, 2011, **471**, 919–923.
12 K. Heine, J. Tenbrink and M. Thöner, *Appl. Phys. Lett.*, 1989, **55**, 2441–2443.
13 K. Sato, T. Hikata, H. Mukai, M. Ueyama, N. Shibuta, T. Kato, T. Masuda, M. Nagata, K. Iwata and T. Mitsui, *IEEE Trans. Magn.*, 1991, **27**, 1231–1238.
14 F. Kametani, J. Jiang, M. Matras, D. Abraimov, E. E. Hellstrom and D. C. Larbalestier, *Sci. Rep.*, 2015, **5**, 8285.
15 S. Jin, R. C. Sherwood, R. B. Van Dover, T. H. Tiefel and D. W. Johnson, *Appl. Phys. Lett.*, 1987, **51**, 203–204.
16 S. Ochiai, K. Hayashi and K. Osamura, *J. Mater. Sci.*, 1990, **25**, 3467–3474.
17 J. Bowker and G. Whitlow, *Supercond. Sci. Technol.*, 1993, **6**, 106–111.
18 L. Chaffron and P. Regnier, *Supercond. Sci. Technol.*, 1991, **4**, S247–S249.
19 K. Osamura, T. Takayama and S. Ochiai, *Supercond. Sci. Technol.*, 1989, **2**, 111–114.
20 X. Wu, Y. Ikeno, K. Kakimoto and S. Horiuchi, *Phys. C*, 1991, **174**, 423–430.
21 K. Osamura, T. Takayama and S. Ochiai, *Cryogenics*, 1990, **29**, 430–433.
22 K. Fischer, G. Leitner, G. Fuchs, M. Schubert, B. Schlobach, A. Gladun and C. Rodig, *Cryogenics*, 1993, **33**, 97–103.
23 P. Paturi, J. Raittila, J.-C. Grivel, H. Huhtinen, B. Seifi, R. Laiho and N. Andersen, *Phys. C*, 2002, **372–376**, 779–781.
24 S. Jin, T. Tiefel, R. Sherwood, M. Davis, G. Kammlott and R. Fastnacht, *Phys. Rev. B: Condens. Matter Mater. Phys.*, 1988, **37**, 7850–7853.
25 M. Murakami, M. Morita, K. Doi and K. Miyamoto, *Jpn. J. Appl. Phys.*, 1989, **28**, 1189–1194.
26 N. D. Kumar, Y. H. Shi, W. Zhai, A. R. Dennis, J. H. Durrell and D. A. Cardwell, *Cryst. Growth Des.*, 2015, **15**, 1472–1780.
27 M. Morita, S. Takebayashi, M. Tanaka, K. Kimura, K. Miyamoto and K. Sawano, *Advances in Superconductivity III*, Springer-Verlag, Tokyo, 1990, pp. 733–736.
28 N. Wu, H. H. Zern and C. Chen, *Phys. C*, 1995, **241**, 198–207.
29 J. L. MacManus-Driscoll, *Adv. Mater.*, 1997, **9**, 457–473.
30 M. O. Rikel, S. Arsac, E. Soileux, J. Ehrenberg, J. Bock, K. Marken, H. Miao, C.-E. Bruzek, S. Pavard, A. Matsumoto, E. E. Hellstrom and L. Motowidlo, *J. Phys.: Conf. Ser.*, 2006, **43**, 51–54.
31 R. E. Loehman, A. P. Tomsia, J. A. Pask and A. H. Carim, *Phys. C*, 1990, **170**, 1–14.
32 D. C. Larbalestier, J. Jiang, U. P. Trociewitz, F. Kametani, C. Scheuerlein, M. Dalban-Canassy, M. Matras, P. Chen, N. C. Craig, P. J. Lee and E. E. Hellstrom, *Nat. Mater.*, 2014, **13**, 375–381.
33 M. Karuna, J. A. Parrell and D. C. Larbalestier, *IEEE Trans. Appl. Supercond.*, 1995, **5**, 1279–1282.